

Resonant diffusion of a gravitactic circle swimmer

Oleksandr Chepizhko¹ and Thomas Franosch¹

¹*Institut für Theoretische Physik, Universität Innsbruck,
Technikerstraße 21A, A-6020, Innsbruck, Austria*

(Dated: January 23, 2023)

We investigate the dynamics of a single chiral active particle subject to an external torque due to the presence of a gravitational field. Our computer simulations reveal an arbitrarily strong increase of the long-time diffusivity of the gravitactic agent when the external torque approaches the intrinsic angular drift. We provide analytic expressions for the mean-square displacement in terms of eigenfunctions and eigenvalues of the noisy-driven-pendulum problem. The pronounced maximum in the diffusivity is then rationalized by the vanishing of the lowest eigenvalues of the Fokker-Planck equation for the angular motion as the rotational diffusion decreases and the underlying classical bifurcation is approached. A simple harmonic-oscillator picture for the barrier-dominated motion provides a quantitative description for the onset of the resonance while its range of validity is determined by the crossover to a critical-fluctuation-dominated regime.

Active particles capable of self-propulsion by converting energy into directed motion have come into research focus and are important from both a fundamental and an applied point of view [1–5]. Examples for active agents include various motile organisms, in particular bacteria [6–8] or algae [9], as well as artificial realizations such as Janus rods [10], spheres [11], or Quincke rollers [12]. Recently, significant advances in our understanding of transport properties of active motion in homogeneous environments [4, 13–18] and in media crowded with obstacles [19–25] have been achieved.

External fields, torques and gradients induce various forms of *taxis* such as chemotaxis [26, 27], magnetotaxis [28, 29], gravitaxis [30], rheotaxis [31], or viscotaxis [32] due to a combination of the persistence of motion and different noise sources [1, 4]. Already the case of a homogeneous force field such as gravity gives rise to counterintuitive dynamics by coupling to the orientational motion. For systems of L -shaped chiral microswimmers [33] and Janus rods [34], mass-anisotropic colloids [35, 36], and microorganisms [30] gravitaxis has been demonstrated experimentally. In particular, these experiments have discovered that chiral active particles subject to a gravitational field can move upwards, which was also supported by simulation studies in bottom-heavy microswimmers [37] and chiral swimmers [38]. Experimental studies of sedimenting active particles revealed an enhancement of diffusivity by activity [39], while an analytical solution for the density profile has been obtained only recently [40]. The sedimentation profile of active particles was also studied in detail in computer simulations and experiments with Janus particles [41] as well as for run-and-tumble particles [42]. Yet, the temporal dynamics and transport properties such as the mean-square displacement and the corresponding diffusivity have not been elucidated in detail.

In this Letter, we demonstrate by computer simulation that gravitaxis of circle swimmers displays resonant diffusivities for small orientational diffusion as the gravita-

tional torque approaches the intrinsic angular drift velocity. We then elaborate a complete analytical solution of gravitactic motion for the model developed by ten Hagen *et al* [33]. A formal expression for the intermediate scattering function, encoding the spatio-temporal motion, is derived. Using a time-dependent perturbative approach we extract the mean drift and the mean-square displacement. Our analytic results reveal that the resonance is encoded in the vanishing of the eigenvalues of the associated Fokker-Planck operator. We rationalize the onset of the resonance within a harmonic approximation and determine the growth of the maximum of the resonance by crossover scaling.

Model.– We rely on the model derived in Ref. [33] for an active chiral particle subject to an external (gravitational) field. The particle moves at constant speed v along a direction $\mathbf{u}(t) := (\cos \vartheta(t), \sin \vartheta(t))^T$ parametrized by a time-dependent angle $\vartheta(t)$ measured from the horizontal

$$\dot{\mathbf{r}}(t) = v\mathbf{u}(t) = v(\cos \vartheta(t), \sin \vartheta(t)). \quad (1)$$

The evolution of $\vartheta(t)$ is governed by two contributions. The external field results in an angle-dependent torque aligning the orientation in a certain direction. The coating of the active particle is such that with this orientation the self-propulsion is horizontal. Additionally, the anisotropy of the particle induces an internal angular drift $\omega > 0$ resulting in the equation of motion

$$\dot{\vartheta}(t) = \omega - \gamma \sin \vartheta(t) + \zeta(t). \quad (2)$$

Here, the torque γ is proportional to the external force and $\zeta(t)$ is a centered Gaussian white noise $\langle \zeta(t)\zeta(t') \rangle = 2D_{\text{rot}}\delta(t-t')$, where D_{rot} is the bare orientational diffusion constant. The equations of motion are rewritten with proper substitutions from Ref. [33], where for simplicity we discard noise terms and additional drift terms due to (anisotropic) translational diffusion in Eq. (1). The neglected terms can be incorporated with little effort but do not change the overall picture of the resonance

phenomenon (see Supplemental Material [43]). Without the external field the model reduces to the free circle swimmer [13, 17, 44, 45], while for $\gamma > 0$ the angular motion corresponds to Brownian motion in a tilted washboard potential [46, 47]. Ignoring the noise in Eq. (2) yields the classical dynamics of an overdamped driven pendulum displaying a saddle-node bifurcation at the critical value $\gamma_c = \omega$ [48]. The mapping of the gravitaxis problem to the noisy driven pendulum constitutes our first result.

Simulation.— The model is encoded in 4 parameters characterizing gravitaxis. We employ $1/\omega$ as fundamental unit of time, while the radius of the circular motion v/ω sets the unit of length. Then γ/ω is the dimensionless torque and D_{rot}/ω quantifies the relative importance of fluctuations. Stochastic simulations are performed and the displacement $\Delta\mathbf{r}(t) := \mathbf{r}(t) - \mathbf{r}(0)$ is monitored in the stationary state. In particular, we extract the mean displacement $\langle\Delta\mathbf{r}(t)\rangle$ and the variance $\text{Var}[\Delta\mathbf{r}(t)] := \langle[\Delta\mathbf{r}(t) - \langle\Delta\mathbf{r}(t)\rangle]^2\rangle$.

In the stationary state the mean displacement grows linearly in time with the average velocity $v(\langle\cos\vartheta(t)\rangle, \langle\sin\vartheta(t)\rangle)$. Since the stationary distribution of the angle $p^{\text{st}}(\vartheta)$ is elementary [49] the mean drift can be readily obtained by quadrature. Here, we recall that without noise, $D_{\text{rot}} = 0$, the orientational angle is locked at $0 < \vartheta_* \leq \pi/2$ with $\sin\vartheta_* = \omega/\gamma$ provided the torque fulfills $\gamma \geq \omega$. If the torque is weaker than the internal drift, $\gamma < \omega$, the angular motion is periodic [48]. Directly at the classical bifurcation, the particle moves upwards against the field [50]. Upon reintroducing the noise the average horizontal motion is suppressed above the bifurcation, while below the fluctuations enable a net drift (see also Fig. S.3 in SM [43]). The drift against the field direction is always suppressed by noise.

The variance $\text{Var}[\Delta\mathbf{r}(t)]$ increases as t^2 for small times, see Fig. 1, where the prefactor decreases drastically as the torque is increased. Below the classical bifurcation characteristic oscillations emerge, similar to the free circle swimmer [17, 51], while for $\gamma > \omega$ the variance increases monotonically. The long-time behavior is diffusive in the presence of noise, $D_{\text{rot}} > 0$, and the diffusion coefficient is enhanced close to the classical bifurcation. The extracted long-time diffusion coefficients $D := \lim_{t \rightarrow \infty} (1/4)d\text{Var}[\Delta\mathbf{r}(t)]/dt$ are displayed in terms of the known diffusivity without external torque [13, 17] $D_0 = v_0^2 D_{\text{rot}}/[2(D_{\text{rot}}^2 + \omega^2)]$ in Fig. 2. Close to the classical bifurcation a resonance emerges that becomes narrower and more pronounced as the noise is decreased.

Theory.— The goal of this part is to provide a theoretical explanation for the found resonance and to derive scaling laws in the vicinity of the classical bifurcation. The dynamical properties are encoded in the propagator $\mathbb{P}(\mathbf{r}, \vartheta, t|\vartheta_0)$, i.e. the conditional probability distribution that the particle has displaced by \mathbf{r} and its instantaneous speed exhibits an orientation ϑ at lag time t given it

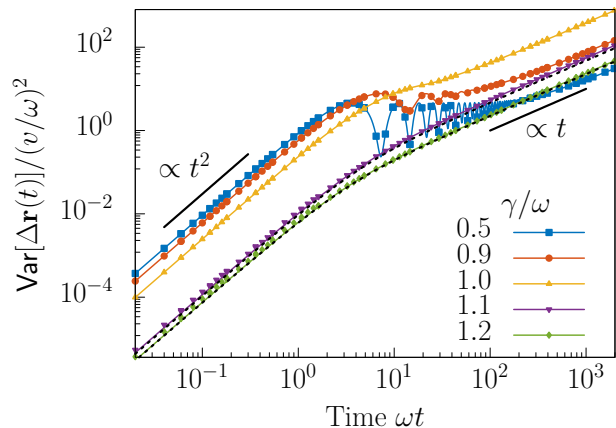


Fig. 1. Time-dependent variance $\text{Var}[\Delta\mathbf{r}(t)]$ on logarithmic scales for a rotational diffusivity of $D_{\text{rot}}/\omega = 0.005^{\text{a}}$ for different torques γ . Symbols correspond to simulation, the solid lines represent the analytic solution. The dotted black lines are evaluated within the harmonic oscillator approximation, Eq. (13b), for $\gamma = 1.1\omega$ and $\gamma = 1.2\omega$. The thick black lines are power laws serving as guide to the eye.

^a Unfortunately, the published version states a wrong value.

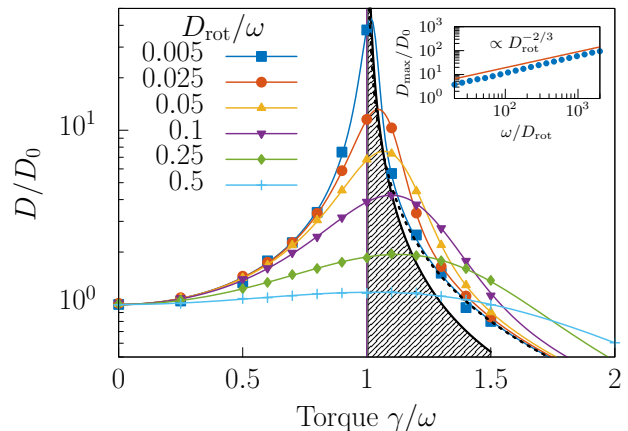


Fig. 2. Resonance of diffusivity. The diffusivity D as a function of the torque γ for different rotational diffusivities D_{rot} . The diffusivity is normalized to the diffusion coefficient of a free circle swimmer $D_0 = v^2 D_{\text{rot}}/[2(D_{\text{rot}}^2 + \omega^2)]$. Symbols correspond to simulation, the full lines are analytical results. The black dotted line corresponds to the harmonic oscillator approximation, Eq. (13b), for $D_{\text{rot}}/\omega = 0.005\omega$. The right boundary of the shaded area corresponds to the parametric curve $\hat{D}_{\text{rot}} := |\gamma/\omega - 1|^{-3/2} D_{\text{rot}}/\omega = \text{const.}$ asymptotically intersecting the maxima of the diffusion coefficients. Inset: Increase of the maximal diffusion coefficient D_{max} for increasing inverse noise $1/D_{\text{rot}}$ on logarithmic scales obtained from theory.^a

^a Unfortunately, this inset contains wrong tic marks in the published version.

started with orientation ϑ_0 . Angles are considered to be 2π -periodic. We focus on its spatial Fourier transform

$\tilde{\mathbb{P}} := \tilde{\mathbb{P}}(\mathbf{k}, \vartheta, t | \vartheta_0) = \int d\mathbf{r} \exp(-i\mathbf{k} \cdot \mathbf{r}) \mathbb{P}(\mathbf{r}, \vartheta, t | \vartheta_0)$ and derive by standard methods [49] the (Fourier transformed) Fokker-Planck equation (see also SM [43])

$$\begin{aligned} \partial_t \tilde{\mathbb{P}} &= -\partial_\vartheta [(\omega - \gamma \sin \vartheta) \tilde{\mathbb{P}}] + D_{\text{rot}} \partial_\vartheta^2 \tilde{\mathbb{P}} - i\mathbf{v}\mathbf{k} \cdot \mathbf{u} \tilde{\mathbb{P}} \\ &=: (\mathcal{L} + \delta\mathcal{L}_{\mathbf{k}}) \tilde{\mathbb{P}}. \end{aligned} \quad (3)$$

Here the operator \mathcal{L} encodes the motion of the angle, while $\delta\mathcal{L}_{\mathbf{k}} = -i\mathbf{v}\mathbf{k} \cdot \mathbf{u}$ describes the coupling to the translational dynamics. The formal solution is thus $\tilde{\mathbb{P}}(\mathbf{k}, \vartheta, t | \vartheta_0) = \exp[(\mathcal{L} + \delta\mathcal{L}_{\mathbf{k}})t] \delta(\vartheta - \vartheta_0)$.

From this quantity the intermediate scattering function (ISF) $F(\mathbf{k}, t) = \langle \exp(-i\mathbf{k} \cdot \Delta\mathbf{r}(t)) \rangle$ is obtained in the stationary state by averaging over the initial angle and integrating over the final one

$$\begin{aligned} F(\mathbf{k}, t) &= \int_0^{2\pi} d\vartheta \int_0^{2\pi} d\vartheta_0 \tilde{\mathbb{P}}(\mathbf{k}, \vartheta, t | \vartheta_0) p^{\text{st}}(\vartheta_0) \\ &= \int_0^{2\pi} d\vartheta \exp[(\mathcal{L} + \delta\mathcal{L}_{\mathbf{k}})t] p^{\text{st}}(\vartheta). \end{aligned} \quad (4)$$

Moments of the displacement can be extracted by a series expansion in the wave vector \mathbf{k}

$$F(\mathbf{k}, t) = 1 - i\mathbf{k} \cdot \langle \Delta\mathbf{r}(t) \rangle - \frac{1}{2} \langle [\mathbf{k} \cdot \Delta\mathbf{r}(t)]^2 \rangle + \dots \quad (5)$$

Here we follow the strategy of Ref. [17] (see also Ref. [52]), solve the eigenvalue problem of the reference system \mathcal{L} , and apply time-dependent perturbation theory for $\delta\mathcal{L}_{\mathbf{k}}$. We denote by $\{|n\rangle : n \in \mathbb{Z}\}$ the standard orthonormal basis in the Hilbert space $L^2[0, 2\pi]$ with real-space representation $\langle \vartheta | n \rangle := \exp(in\vartheta) / \sqrt{2\pi}$. In this basis \mathcal{L} is represented in terms of its matrix elements [49]

$$\begin{aligned} \mathcal{L}_{mn} &= \langle m | \mathcal{L} n \rangle := \int_0^{2\pi} \frac{d\vartheta}{2\pi} e^{-im\vartheta} \mathcal{L} e^{in\vartheta} \\ &= (-D_{\text{rot}} m^2 - im\omega) \delta_{mn} + \frac{\gamma}{2} m (\delta_{m, n+1} - \delta_{m, n-1}). \end{aligned} \quad (6)$$

In particular, the matrix representation is non-Hermitian and tridiagonal due to the torque. Right and left eigenstates $\mathcal{L}|r_\lambda\rangle = -\lambda|r_\lambda\rangle$, $\mathcal{L}^\dagger|l_\lambda\rangle = -\lambda^*|l_\lambda\rangle$ are readily obtained by numerically diagonalizing the matrix, Eq. (SM16), yielding the expansion coefficients $\langle n|r_\lambda\rangle$, $\langle l_\lambda|n\rangle$ as right and left eigenvector of the matrix \mathcal{L}_{mn} . The corresponding real-space representation is obtained by expansion $r_\lambda(\vartheta) = \sum_{n \in \mathbb{Z}} \langle \vartheta | n \rangle \langle n | r_\lambda \rangle$. By conservation of probability $\lambda = 0$ is an eigenvalue and the real-space representation of the associated eigenstates are $r_0(\vartheta) = p^{\text{st}}(\vartheta)$ and $l_0(\vartheta) = 1$. Comparing with Eq. (SM11) we find the compact expression for the ISF

$$F(\mathbf{k}, t) = \langle l_0 | \exp[(\mathcal{L} + \delta\mathcal{L}_{\mathbf{k}})t] r_0 \rangle. \quad (7)$$

Since $\delta\mathcal{L}_{\mathbf{k}} = -i\mathbf{v}\mathbf{k} \cdot \mathbf{u}$, time-dependent perturbation theory (Born series) [53]

$$\begin{aligned} e^{(\mathcal{L} + \delta\mathcal{L}_{\mathbf{k}})t} &= e^{\mathcal{L}t} + \int_0^t ds e^{\mathcal{L}(t-s)} \delta\mathcal{L}_{\mathbf{k}} e^{\mathcal{L}s} \\ &\quad + \int_0^t ds \int_0^s du e^{\mathcal{L}(t-s)} \delta\mathcal{L}_{\mathbf{k}} e^{\mathcal{L}(s-u)} \delta\mathcal{L}_{\mathbf{k}} e^{\mathcal{L}u} \\ &\quad + O(\delta\mathcal{L}_{\mathbf{k}})^3, \end{aligned} \quad (8)$$

directly yields the moments of the series expansion in \mathbf{k} as in Eq. (5). In particular, expanding to second order in \mathbf{k} and squeezing in the completeness relation $\sum_\lambda |r_\lambda\rangle \langle l_\lambda| = \mathbb{1}$, the time integrals can be formally performed (see also SM [43]). Then we read off the mean drift velocity and the variance along the direction $\mathbf{n} := \mathbf{k}/k$

$$\mathbf{n} \cdot \frac{d}{dt} \langle \Delta\mathbf{r}(t) \rangle = \frac{1}{k} \langle l_0 | \delta\mathcal{L}_{\mathbf{k}} r_0 \rangle, \quad (9a)$$

$$\text{Var}[\mathbf{n} \cdot \Delta\mathbf{r}(t)] = \frac{2}{k^2} \sum_{\lambda \neq 0} \frac{1 - \lambda t - e^{-\lambda t}}{\lambda^2} \langle l_0 | \delta\mathcal{L}_{\mathbf{k}} r_\lambda \rangle \langle l_\lambda | \delta\mathcal{L}_{\mathbf{k}} r_0 \rangle, \quad (9b)$$

and infer the associated long-time diffusion coefficient

$$D_{\mathbf{n}} = \frac{-1}{k^2} \sum_{\lambda \neq 0} \frac{1}{\lambda} \langle l_0 | \delta\mathcal{L}_{\mathbf{k}} r_\lambda \rangle \langle l_\lambda | \delta\mathcal{L}_{\mathbf{k}} r_0 \rangle. \quad (10)$$

The analytical expressions for the total variances as well as the corresponding diffusion coefficient perfectly match the simulations, see Figs. 1 and 2. The exact expressions in terms of eigenfunctions and eigenvalues suggest that at resonance the eigenvalues become smaller and smaller as the rotational diffusion coefficient is decreased, which is confirmed by numerical diagonalization (see SM [43]).

To gain further analytical insight, we evaluate Eqs. (9) and (10) within a harmonic approximation for the motion close to the classical fixed point ϑ_* . For small $D_{\text{rot}} \ll \omega$ and well above the bifurcation the fluctuations are anticipated to be small and the corresponding linearized Langevin equation reads

$$\dot{\vartheta}(t) = -\frac{1}{\tau} [\vartheta(t) - \vartheta_*] + \zeta(t), \quad (11)$$

with vanishing relaxation rate $1/\tau = \sqrt{\gamma^2 - \omega^2} \rightarrow 0$ as $\gamma \downarrow \omega$. The associated eigenvalues of the overdamped harmonic oscillator are then simply $\lambda_n = n/\tau$, $n \in \mathbb{N}_0$ [49], and indeed they approach zero for $\gamma \downarrow 0$ (see also SM [43]).

To leading order we replace the perturbing operator $\delta\mathcal{L}_{\mathbf{k}}$ by the complex number $i\mathbf{v}\mathbf{k} \cdot \mathbf{u}_*$ with the fixed orientation $\mathbf{u}_* = (\cos \vartheta_*, \sin \vartheta_*)$. In this approximation, the drift velocity, is non-fluctuating and assumes its classical value. In the same approximation the variance and diffusion coefficient vanish by orthogonality of the eigenstates, consistent with a purely deterministic and non-chaotic

motion. To leading non-trivial order we replace

$$\delta\mathcal{L}_{\mathbf{k}} \simeq iv\mathbf{k} \cdot \mathbf{u}_* + (\vartheta - \vartheta_*) \left. \frac{\partial}{\partial\vartheta} \delta\mathcal{L}_{\mathbf{k}} \right|_{\vartheta=\vartheta_*}. \quad (12)$$

Then within the harmonic oscillator approximation, also the off-diagonal matrix elements can be evaluated analytically, in particular, their magnitude is proportional to the angular oscillator width $\langle(\vartheta - \vartheta_*)^2\rangle = \sqrt{D_{\text{rot}}\tau}$ (see SM [43] for details). Furthermore, the angular position operator $\vartheta - \vartheta_*$ induces only non-vanishing transition matrix element in Eqs. (9b),(10) coupling the ground state to the first excited state. Therefore the sums reduce to a single term and we find the compact expressions

$$\text{Var}[\mathbf{n} \cdot \Delta\mathbf{r}(t)] \simeq 2D_{\mathbf{n}}\tau \left(\frac{t}{\tau} - 1 + e^{-t/\tau} \right), \quad (13a)$$

$$D_{\mathbf{n}} \simeq (v\tau)^2 D_{\text{rot}} (n_x \sin \vartheta_* - n_y \cos \vartheta_*)^2. \quad (13b)$$

Within the harmonic oscillator approximation the variance is strictly proportional to D_{rot} suggesting that for sufficiently small orientational fluctuations the curves in Figs. 1 and 2 should approach a master curve. The corresponding curves are included in Figs. 1 and 2 as black dotted lines and are in quantitative agreement for small $D_{\text{rot}} \ll \omega$ and $\gamma > \omega$ not too close to the bifurcation. The emergence of the resonance is thus rationalized in terms of the softening of the harmonic relaxation rate $1/\tau \rightarrow 0$ as the bifurcation is approached.

The harmonic picture suggests that the diffusion coefficient becomes infinite directly at the bifurcation while the simulation and the full analytic expression predict a rounding with a maximal diffusivity. The picture of the harmonic oscillator should hold provided the barrier is sufficiently high such that Kramers' escape rate [49] is much smaller than the harmonic relaxation rate. In terms of the effective potential $D_{\text{rot}}U(\vartheta)/k_B T = -\omega\vartheta - \gamma \cos \vartheta$ the barrier height $\Delta U := U(\pi - \vartheta_*) - U(\vartheta_*)$ reduces to

$$\frac{\Delta U}{k_B T} = \frac{4\sqrt{2}}{3} \frac{\omega}{D_{\text{rot}}} \epsilon^{3/2} [1 + O(\epsilon)], \quad (14)$$

where we introduced the separation parameter $\epsilon := (\gamma - \omega)/\omega$ for the distance to the bifurcation (see SM [43] for details). This observation suggests introducing the reduced rotational diffusion coefficient $\hat{D}_{\text{rot}} := |\epsilon|^{-3/2} D_{\text{rot}}/\omega$ such that for $\hat{D}_{\text{rot}} \ll 1, \epsilon > 0$ the harmonic approximation holds, while for $\hat{D}_{\text{rot}} \gg 1$ the barrier can be crossed readily by fluctuations and the precise height of the barrier should be irrelevant. By matching the critical fluctuation to the harmonic oscillator we predict that the maximal diffusivity should occur at $\hat{D}_{\text{rot}} = O(1)$ or $D_{\text{rot}} \propto |\epsilon|^{3/2}$. For small $\epsilon >$, the relaxation time diverges as $\tau \propto |\epsilon|^{-1/2}$ and from Eq. (13b) we infer the scaling law for the maximal diffusivity

$$D_{\text{max}}/D_0 \propto |\epsilon|^{-1} \propto D_{\text{rot}}^{-2/3} \quad \text{for } D_{\text{rot}} \rightarrow 0, \quad (15)$$

where we used that $D_0 \propto D_{\text{rot}}$ as $D_{\text{rot}} \rightarrow 0$. The numerical values nicely follow the prediction asymptotically as shown in Fig. 2.

Summary and Conclusion.— We have demonstrated that the long-time translational diffusivity of a chiral active Brownian particle displays a resonance for the external torque approaching the intrinsic angular drift. The resonance originates from an underlying bifurcation of the classical driven pendulum. There are certain similarities with the giant diffusion in tilted washboard potentials [46], yet our approach of decomposition into eigenfunctions is rather complementary and allows calculating the entire time-dependence of low-order moments and is in spirit closer to Ref. [47]. The connection of the resonance to the vanishing low-lying eigenvalues is uncovered and an intuitive picture in terms of a competition between barrier-dominated and critical-fluctuation-dominated regime is developed.

The harmonic approximation is surprisingly accurate for the variance as well as for the diffusivity, despite ignoring the rare activation processes over the barrier. We conclude that far above the bifurcation, the orientation performs only small fluctuations most of the time close to the minimum of the effective potential. Then the diffusion coefficient for the translational diffusion remains also small. Yet, approaching the bifurcation these fluctuations become more significant as the confining angular potentials becomes softer yielding a significant enhancement of the diffusivity. For too large angular fluctuations the harmonic approximation breaks down as barrier-crossing events become important. After such barrier crossings the orientation quickly completes a full turn until getting stuck again. From the accurateness of the harmonic oscillator description we conclude that these fast events do not significantly contribute to the diffusivity. The essence of the resonance is thus due to the enhancement of small fluctuations as provided by the orientational diffusion coefficient exploring a softening potential as the bifurcation is approached.

Our theoretical work makes detailed predictions for active motion of chiral agents in external fields that can be tested in experiments, both for artificial and biological asymmetric microswimmers. The method is readily extended to calculate higher moments such as the skewness, the non-Gaussian parameter, or the complete intermediate scattering function. While we explicitly considered gravitaxis, the underlying equations are rather generic and the analysis and methods presented should transfer with suitable adjustments to other forms of *taxis* at the microscale such as durotaxis [54], chemotaxis [27], thermotaxis [55], or topotaxis [56]. Also, the results could be valuable for the transport rigid polymer solutions in a flow near a wall [57].

The resonance is of interest not only for single-particle transport in external fields, but also has implications for the collective motion of chiral active particles with align-

ment interactions [58–61] provided effective mean-field equations can be derived [62–65] which would be similar in structure to the equations of motion studied here.

Last our work has theoretical ramifications on the interplay of the critical slowing down of classical transport close to bifurcations and their smearing by random fluctuations. The evolution of the eigenspectrum also for other bifurcations, including the pitchfork or transcritical bifurcations, should be relevant for various branches of science, such as the physics of the Josephson junction [48] or collective (Kuramoto) synchronization [66].

Acknowledgments.— We thank Christina Kurzthaler for constructive criticism on the manuscript. OC is supported by the Austrian Science Fund (FWF): M 2450-NBL. TF acknowledges funding by FWF: P 35580-N. The computational results presented have been achieved in part using the HPC infrastructure LEO of the University of Innsbruck.

-
- [1] P. Romanczuk, M. Bär, W. Ebeling, B. Lindner, and L. Schimansky-Geier, Active Brownian particles, *The European Physical Journal Special Topics* **202**, 1 (2012).
- [2] J. Elgeti, R. G. Winkler, and G. Gompper, Physics of microswimmers—single particle motion and collective behavior: a review, *Reports on Progress in Physics* **78**, 056601 (2015).
- [3] C. Bechinger, R. Di Leonardo, H. Löwen, C. Reichhardt, G. Volpe, and G. Volpe, Active particles in complex and crowded environments, *Rev. Mod. Phys.* **88**, 045006 (2016).
- [4] A. Zöttl and H. Stark, Emergent behavior in active colloids, *Journal of Physics: Condensed Matter* **28**, 253001 (2016).
- [5] G. Gompper, R. G. Winkler, T. Speck, A. Solon, C. Nardin, F. Peruani, H. Löwen, R. Golestanian, U. B. Kaupp, L. Alvarez, T. Kiørboe, E. Lauga, W. C. K. Poon, A. DeSimone, S. Muiños-Landin, A. Fischer, N. A. Söker, F. Cichos, R. Kapral, P. Gaspard, M. Ripoll, F. Sagues, A. Doostmohammadi, J. M. Yeomans, I. S. Aranson, C. Bechinger, H. Stark, C. K. Hemelrijk, F. J. Nedelec, T. Sarkar, T. Aryaksama, M. Lacroix, G. Duclos, V. Yashunsky, P. Silberzan, M. Arroyo, and S. Kale, The 2020 motile active matter roadmap, *Journal of Physics: Condensed Matter* **32**, 193001 (2020).
- [6] H. C. Berg and D. A. Brown, Chemotaxis in *escherichia coli* analysed by three-dimensional tracking, *Nature* **239**, 500 (1972).
- [7] H. Berg and L. Turner, Chemotaxis of bacteria in glass capillary arrays. *escherichia coli*, motility, microchannel plate, and light scattering, *Biophysical Journal* **58**, 919 (1990).
- [8] E. Lauga, W. R. DiLuzio, G. M. Whitesides, and H. A. Stone, Swimming in circles: Motion of bacteria near solid boundaries, *Biophysical Journal* **90**, 400 (2006).
- [9] S. S. Merchant *et al.*, The *Chlamydomonas* genome reveals the evolution of key animal and plant functions, *Science* **318**, 245 (2007).
- [10] A. T. Brown, I. D. Vladescu, A. Dawson, T. Vissers, J. Schwarz-Linek, J. S. Lintuvuori, and W. C. K. Poon, Swimming in a crystal, *Soft Matter* **12**, 131 (2016).
- [11] I. Buttinoni, G. Volpe, F. Kümmel, G. Volpe, and C. Bechinger, Active Brownian motion tunable by light, *Journal of Physics: Condensed Matter* **24**, 284129 (2012).
- [12] A. Bricard, J.-B. Caussin, N. Desreumaux, O. Dauchot, and D. Bartolo, Emergence of macroscopic directed motion in populations of motile colloids, *Nature* **503**, 95 (2013).
- [13] S. van Teeffelen and H. Löwen, Dynamics of a Brownian circle swimmer, *Physical Review E* **78**, 020101(R) (2008).
- [14] F. J. Sevilla and L. A. Gómez Nava, Theory of diffusion of active particles that move at constant speed in two dimensions, *Physical Review E* **90**, 022130 (2014).
- [15] C. Kurzthaler, S. Leitmann, and T. Franosch, Intermediate scattering function of an anisotropic active Brownian particle, *Scientific Reports* **6**, 36702 (2016).
- [16] J. Toner, H. Löwen, and H. H. Wensink, Following fluctuating signs: Anomalous active superdiffusion of swimmers in anisotropic media, *Physical Review E* **93**, 062610 (2016).
- [17] C. Kurzthaler and T. Franosch, Intermediate scattering function of an anisotropic Brownian circle swimmer, *Soft Matter* **13**, 6396 (2017).
- [18] C. Kurzthaler, C. Devailly, J. Arlt, T. Franosch, W. C. K. Poon, V. A. Martinez, and A. T. Brown, Probing the spatiotemporal dynamics of catalytic janus particles with single-particle tracking and differential dynamic microscopy, *Physical Review Letters* **121**, 078001 (2018).
- [19] G. Volpe, I. Buttinoni, D. Vogt, H.-J. Kümmerer, and C. Bechinger, Microswimmers in patterned environments, *Soft Matter* **7**, 8810 (2011).
- [20] O. Chepizhko and F. Peruani, Diffusion, subdiffusion, and trapping of active particles in heterogeneous media, *Physical Review Letters* **111**, 160604 (2013).
- [21] D. Takagi, J. Palacci, A. B. Braunschweig, M. J. Shelley, and J. Zhang, Hydrodynamic capture of microswimmers into sphere-bound orbits, *Soft Matter* **10**, 1784 (2014).
- [22] M. Zeitz, K. Wolff, and H. Stark, Active Brownian particles moving in a random Lorentz gas, *The European Physical Journal E* **40**, 23 (2017).
- [23] C. Reichhardt and C. J. Olson Reichhardt, Active matter transport and jamming on disordered landscapes, *Physical Review E* **90**, 012701 (2014).
- [24] C. Reichhardt and C. J. O. Reichhardt, Negative differential mobility and trapping in active matter systems, *Journal of Physics: Condensed Matter* **30**, 015404 (2018).
- [25] O. Chepizhko and T. Franosch, Ideal circle microswimmers in crowded media, *Soft Matter* **15**, 452 (2019).
- [26] B. Liebchen and H. Löwen, Synthetic chemotaxis and collective behavior in active matter, *Accounts of Chemical Research* **51**, 2982 (2018).
- [27] H. D. Vuijk, H. Merlitz, M. Lang, A. Sharma, and J.-U. Sommer, Chemotaxis of cargo-carrying self-propelled particles, *Physical Review Letters* **126**, 208102 (2021).
- [28] K. Érglis, Q. Wen, V. Ose, A. Zeltins, A. Sharipo, P. A. Janmey, and A. Cēbers, Dynamics of magnetotactic bacteria in a rotating magnetic field, *Biophysical Journal* **93**, 1402 (2007).
- [29] D. Faivre and D. Schüler, Magnetotactic bacteria and magnetosomes, *Chemical Reviews* **108**, 4875 (2008).
- [30] A. M. Roberts, Mechanisms of gravitaxis in *chlamydomonas*, *The Biological Bulletin* **210**, 78 (2006); The

- mechanics of gravitaxis in Paramecium, *Journal of Experimental Biology* **213**, 4158 (2010).
- [31] A. J. T. M. Mathijssen, N. Figueroa-Morales, G. Junot, É. Clément, A. Lindner, and A. Zöttl, Oscillatory surface rheotaxis of swimming *E. coli* bacteria, *Nature Communications* **10** (2019).
- [32] B. Liebchen, P. Monderkamp, B. ten Hagen, and H. Löwen, Viscotaxis: Microswimmer navigation in viscosity gradients, *Physical Review Letters* **120**, 208002 (2018).
- [33] B. ten Hagen, F. Kümmel, R. Wittkowski, D. Takagi, H. Löwen, and C. Bechinger, Gravitaxis of asymmetric self-propelled colloidal particles, *Nature Communications* **5**, 4829 (2014).
- [34] Q. Brosseau, F. B. Usabiaga, E. Lushi, Y. Wu, L. Ristroph, M. D. Ward, M. J. Shelley, and J. Zhang, Metallic microswimmers driven up the wall by gravity, *Soft Matter* **17**, 6597 (2021).
- [35] A. I. Campbell, R. Wittkowski, B. ten Hagen, H. Löwen, and S. J. Ebbens, Helical paths, gravitaxis, and separation phenomena for mass-anisotropic self-propelling colloids: Experiment versus theory, *The Journal of Chemical Physics* **147**, 084905 (2017).
- [36] D. P. Singh, W. E. Uspal, M. N. Popescu, L. G. Wilson, and P. Fischer, Photogravitactic microswimmers, *Advanced Functional Materials* **28**, 1706660 (2018).
- [37] F. Rühle and H. Stark, Emergent collective dynamics of bottom-heavy squirmers under gravity, *The European Physical Journal E* **43** (2020).
- [38] F. Fadda, J. J. Molina, and R. Yamamoto, Dynamics of a chiral swimmer sedimenting on a flat plate, *Physical Review E* **101**, 052608 (2020).
- [39] J. Palacci, C. Cottin-Bizonne, C. Ybert, and L. Bocquet, Sedimentation and effective temperature of active colloidal suspensions, *Physical Review Letters* **105**, 088304 (2010).
- [40] J. Vachier and M. G. Mazza, Dynamics of sedimenting active Brownian particles, *The European Physical Journal E* **42** (2019).
- [41] F. Ginot, A. Solon, Y. Kafri, C. Ybert, J. Tailleur, and C. Cottin-Bizonne, Sedimentation of self-propelled Janus colloids: polarization and pressure, *New Journal of Physics* **20**, 115001 (2018).
- [42] R. W. Nash, R. Adhikari, J. Tailleur, and M. E. Cates, Run-and-tumble particles with hydrodynamics: Sedimentation, trapping, and upstream swimming, *Physical Review Letters* **104**, 258101 (2010).
- [43] See Supplemental Material at [URL] for details for the mapping to the noisy driven pendulum, and additional figures for the mean drift and the diffusivity in the presence of additional translational diffusion. The Supplemental Material includes Ref [44].
- [44] B. M. Friedrich and F. Jülcher, The stochastic dance of circling sperm cells: sperm chemotaxis in the plane, *New Journal of Physics* **10**, 123025 (2008).
- [45] H. Löwen, Chirality in microswimmer motion: From circle swimmers to active turbulence, *The European Physical Journal Special Topics* **225**, 2319 (2016).
- [46] P. Reimann, C. Van den Broeck, H. Linke, P. Hänggi, J. M. Rubi, and A. Pérez-Madrid, Giant acceleration of free diffusion by use of tilted periodic potentials, *Physical Review Letters* **87**, 010602 (2001); Diffusion in tilted periodic potentials: Enhancement, universality, and scaling, *Physical Review E* **65**, 031104 (2002).
- [47] N. J. López-Alamilla, M. W. Jack, and K. J. Challis, Enhanced diffusion and the eigenvalue band structure of Brownian motion in tilted periodic potentials, *Physical Review E* **102**, 042405 (2020).
- [48] S. H. Strogatz, *Nonlinear dynamics and chaos: with applications to physics, biology, chemistry, and engineering*, 2nd ed. (CRC press, 2018).
- [49] H. Risken, *The Fokker-Planck Equation* (Springer Berlin Heidelberg, 1989).
- [50] This will somewhat change upon reinstating the terms due to translational diffusion which we ignore here.
- [51] F. Kümmel, B. ten Hagen, R. Wittkowski, I. Buttinoni, R. Eichhorn, G. Volpe, H. Löwen, and C. Bechinger, Circular motion of asymmetric self-propelling particles, *Physical Review Letters* **110**, 198302 (2013).
- [52] A. Lapolla, D. Hartich, and A. c. v. Godec, Spectral theory of fluctuations in time-average statistical mechanics of reversible and driven systems, *Phys. Rev. Research* **2**, 043084 (2020).
- [53] J. Sakurai and J. Napolitano, *Modern quantum mechanics*. San Fransico (CA: Addison-Wesley, 2011).
- [54] C.-M. Lo, H.-B. Wang, M. Dembo, and Y. li Wang, Cell movement is guided by the rigidity of the substrate, *Biophysical Journal* **79**, 144 (2000).
- [55] S. Auschra, A. Bregulla, K. Kroy, and F. Cichos, Thermo-taxis of Janus particles, *The European Physical Journal E* **44** (2021).
- [56] K. Schakenraad, L. Ravazzano, N. Sarkar, J. A. J. Woutergem, R. M. H. Merks, and L. Giomi, Topotaxis of active Brownian particles, *Physical Review E* **101**, 032602 (2020).
- [57] J. Park, J. M. Bricker, and J. E. Butler, Cross-stream migration in dilute solutions of rigid polymers undergoing rectilinear flow near a wall, *Physical Review E* **76**, 10.1103/physreve.76.040801 (2007).
- [58] B. Liebchen and D. Levis, Collective behavior of chiral active matter: Pattern formation and enhanced flocking, *Physical Review Letters* **119**, 058002 (2017).
- [59] D. Levis and B. Liebchen, Micro-flock patterns and macro-clusters in chiral active Brownian disks, *Journal of Physics: Condensed Matter* **30**, 084001 (2018).
- [60] B. Ventejou, H. Chaté, R. Montagne, and X. Q. Shi, Susceptibility of orientationally ordered active matter to chirality disorder, *Physical Review Letters* **127**, 238001 (2021).
- [61] Q.-L. Lei, M. P. Ciamarra, and R. Ni, Nonequilibrium strongly hyperuniform fluids of circle active particles with large local density fluctuations, *Science Advances* **5**, 10.1126/sciadv.aau7423 (2019).
- [62] A. A. Chepizhko and V. L. Kulinskii, On the relation between Vicsek and Kuramoto models of spontaneous synchronization, *Physica A: Statistical Mechanics and its Applications* **389**, 5347 (2010).
- [63] F. Peruani, A. Deutsch, and M. Bär, A mean-field theory for self-propelled particles interacting by velocity alignment mechanisms, *The European Physical Journal Special Topics* **157**, 111 (2008).
- [64] J. A. Pimentel, M. Aldana, C. Huepe, and H. Larralde, Intrinsic and extrinsic noise effects on phase transitions of network models with applications to swarming systems, *Physical Review E* **77**, 061138 (2008).
- [65] F. Bolley, J. A. Cañizo, and J. A. Carrillo, Mean-field limit for the stochastic vicsek model, *Applied Mathematics Letters* **25**, 339 (2012).

- [66] J. A. Acebrón, L. L. Bonilla, C. J. Pérez Vicente, F. Ritort, and R. Spigler, The Kuramoto model: A simple paradigm for synchronization phenomena, *Rev. Mod. Phys.* **77**, 137 (2005).
- [67] B. U. Felderhof, Comment on “Circular motion of asymmetric self-propelling particles”, *Physical Review Letters* **113** (2014).
- [68] F. Kümmel, B. ten Hagen, R. Wittkowski, D. Takagi, I. Buttinoni, R. Eichhorn, G. Volpe, H. Löwen, and C. Bechinger, Kümmel et al. Reply:, *Physical Review Letters* **113**, 029802 (2014).
- [69] Since \mathcal{L} is non-Hermitian one has to carefully indicate whether operators act to the right or the left.

SUPPLEMENTAL MATERIAL

SIMPLIFYING THE EQUATIONS OF MOTION AND MAPPING TO THE NOISY DRIVEN PENDULUM

The stochastic equations of motion for an asymmetric circle swimmer in the presence of an external (gravitational) field were proposed by ten Hagen *et al.* in Ref. [1]. The goal of this section is to show that the model greatly simplifies upon a simple rotation to the principal axis of the system. Furthermore the essence of gravitaxis can be discussed by discarding additional terms connected to translational diffusion and the associated noise. In this approximation the model reduces to the paradigmatic noise driven pendulum. Explicitly the equations of motion of Ref. [1] read

$$\dot{\mathbf{r}}(t) = \frac{P^*}{b} [\mathbf{D}_T(t) \cdot \mathbf{u}^\perp(t) + \ell \mathbf{D}_C(t)] + \beta \mathbf{D}_T(t) \cdot \mathbf{F} + \boldsymbol{\zeta}_r(t), \quad (\text{SM1a})$$

$$\dot{\varphi}(t) = \frac{P^*}{b} [\ell D_{\text{rot}} + \mathbf{D}_C(t) \cdot \mathbf{u}^\perp(t)] + \beta \mathbf{D}_C(t) \cdot \mathbf{F} + \zeta(t), \quad (\text{SM1b})$$

for the time-dependent position $\mathbf{r}(t)$ and the orientational angle $\varphi(t)$ of the particle. The two unit vectors $\mathbf{u}^\parallel(t) = (\cos \varphi(t), \sin \varphi(t))$ and $\mathbf{u}^\perp(t) = (-\sin \varphi(t), \cos \varphi(t))$ are associated with the orientational angle $\varphi(t)$, see Fig. SM1 for illustration. Furthermore, $\mathbf{F} = (0, -mg \sin \alpha) = (0, -F)$ denotes the gravitational force, $\mathbf{D}_T(t) = D_\parallel \mathbf{u}^\parallel(t) \otimes \mathbf{u}^\parallel(t) + D_\perp^\perp [\mathbf{u}^\parallel \otimes \mathbf{u}^\perp(t) + \mathbf{u}^\perp(t) \otimes \mathbf{u}^\parallel(t)] + D_\perp \mathbf{u}_\perp(t) \otimes \mathbf{u}_\perp(t)$, $\mathbf{D}_C(t) = D_C^\parallel \mathbf{u}^\parallel(t) + D_C^\perp \mathbf{u}^\perp(t)$ encodes the translational diffusion and the translation-rotation coupling[2], $\beta = 1/k_B T$ refers to the inverse (effective) temperature, ℓ and b are characteristic lengths, and P^* is the strength of the self propulsion. Last, $\boldsymbol{\zeta}_r, \zeta_\varphi$ are independent centered Gaussian white noises of variance $\langle \boldsymbol{\zeta}_r(t) \otimes \boldsymbol{\zeta}_r(t') \rangle = 2\mathbf{D}_T(t)\delta(t-t')$, $\langle \zeta(t)\zeta(t') \rangle = 2D_{\text{rot}}\delta(t-t')$ respectively.

Without restriction we assume the unit vectors $\mathbf{u}^\parallel(t), \mathbf{u}^\perp(t)$ to be chosen as the principal axes of the the tensor \mathbf{D}_T . In this frame the tensor becomes diagonal and we henceforth ignore the couplings D_\perp^\perp and refer to the orientation of the particle as the angle of the principal axis of the larger eigenvalue D^\parallel with respect to some space-fixed reference axis.

Evaluating the scalar products in the angular equation of motion yields

$$\dot{\varphi}(t) = \frac{P^*}{b} (\ell D_{\text{rot}} + D_C^\perp) - \beta F (D_C^\parallel \cos \varphi(t) + D_C^\perp \sin \varphi(t)) + \zeta(t). \quad (\text{SM2})$$

Using trigonometric addition formulas this simplifies to

$$\dot{\varphi}(t) = \omega - \gamma \sin(\varphi(t) - \varphi_H) + \zeta(t), \quad (\text{SM3})$$

with the angular drift velocity ω , angular driving γ , and the *Hall angle* φ_H given by

$$\omega = \frac{P^*}{b} (\ell D_{\text{rot}} + D_C^\perp), \quad \gamma = \beta F \sqrt{(D_C^\parallel)^2 + (D_C^\perp)^2}, \quad (\text{SM4a})$$

$$\sin \varphi_H = -\beta F D_C^\perp / \gamma, \quad \cos \varphi_H = \beta F D_C^\parallel / \gamma. \quad (\text{SM4b})$$

Similarly the translational equation of motion simplifies to

$$\begin{aligned} \dot{\mathbf{r}}(t) &= \frac{P^*}{b} [D_\perp \mathbf{u}^\perp(t) + \ell D_C^\parallel \mathbf{u}^\parallel(t) + \ell D_C^\perp \mathbf{u}^\perp(t)] + \beta D_\parallel [\mathbf{F} \cdot \mathbf{u}^\parallel(t)] \mathbf{u}^\parallel(t) \cos \varphi(t) + \beta D_\perp [\mathbf{F} \cdot \mathbf{u}^\parallel(t)] \mathbf{u}^\perp(t) \cos \varphi(t) + \boldsymbol{\zeta}_r \\ &=: v \begin{pmatrix} \cos(\varphi(t) - \varphi_H) \\ \sin(\varphi(t) - \varphi_H) \end{pmatrix} + v_1 \begin{pmatrix} -\sin \varphi(t) \\ \cos \varphi(t) \end{pmatrix} - v_2 \begin{pmatrix} \sin(2\varphi(t)) \\ \cos(2\varphi(t)) \end{pmatrix} - v_3 \begin{pmatrix} 0 \\ 1 \end{pmatrix} + \boldsymbol{\zeta}_r \\ &=: \mathbf{V}(t) + \boldsymbol{\zeta}_r(t), \end{aligned} \quad (\text{SM5})$$

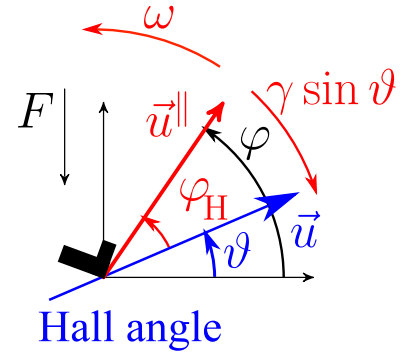


Fig. SM1. a) Illustration of the coordinate system used. The orientation of the principal axis of the particle is along $\mathbf{u}^\parallel = (\cos \varphi, \sin \varphi)$, the drift velocity $\mathbf{u} = (\cos \vartheta, \sin \vartheta)$ is tilted by the Hall angle φ_H to the particle's principal axes. The torque φ_H tends to align the particle's direction with the Hall direction while the intrinsic angular drift rotates the direction counter-clockwise.

with $v = P^* \ell \gamma / b \beta F$, $v_1 = P^* D_\perp / b$, $v_2 = \beta F (D_\parallel - D_\perp) / 2$, $v_3 = \beta F (D_\parallel + D_\perp) / 2$. Without circular motion and ignoring both rotational as well as translational thermal fluctuations, a stationary solution with $\varphi(t) = \varphi_H$ exists, the particle moves with constant velocity perpendicularly to the external field, see Fig. SM1. We abbreviate $\vartheta(t) = \varphi(t) - \varphi_H$ and find the e.o.m.

$$\dot{\vartheta}(t) = \omega - \gamma \sin \vartheta(t) + \zeta(t), \quad \dot{\mathbf{r}}(t) = \mathbf{V}(t) + \boldsymbol{\zeta}_r(t), \quad (\text{SM6})$$

with independent centered Gaussian white noise characterized by $\langle \zeta(t) \zeta(t') \rangle = 2D_{\text{rot}} \delta(t - t')$, $\langle \boldsymbol{\zeta}_r(t) \otimes \boldsymbol{\zeta}_r(t') \rangle = 2D_T(t) \delta(t - t')$. Ignoring the terms induced by translational diffusion, the e.o.m. for the translational motion simplifies to the one discussed in the main text

$$\dot{\vartheta}(t) = \omega - \gamma \sin \vartheta(t) + \zeta(t), \quad \dot{\mathbf{r}}(t) = v \mathbf{u}(t) := v \begin{pmatrix} \cos \vartheta(t) \\ \sin \vartheta(t) \end{pmatrix}. \quad (\text{SM7})$$

FOKKER-PLANCK EQUATION, INTERMEDIATE SCATTERING FUNCTION AND PERTURBATION THEORY

Fokker-Planck equation

By standard techniques [3] one derives the Fokker-Planck equation for the conditional probability density $\mathbb{P} = \mathbb{P}(\mathbf{r}, \vartheta, t | \vartheta_0)$ to find the particle at speed orientation ϑ and displaced by \mathbf{r} at time t given the orientation at time $t = 0$ is prescribed to ϑ_0 :

$$\partial_t \mathbb{P} = -\partial_\vartheta [(\omega - \gamma \sin \vartheta) \mathbb{P}] + D_{\text{rot}} \partial_\vartheta^2 \mathbb{P} - \frac{\partial}{\partial \mathbf{r}} \cdot (\mathbf{V} \mathbb{P}) + \frac{\partial}{\partial \mathbf{r}} \cdot \left(D_T \cdot \frac{\partial}{\partial \mathbf{r}} \mathbb{P} \right). \quad (\text{SM8})$$

The initial condition is provided by $\mathbb{P}(\mathbf{r}, \vartheta, t = 0 | \vartheta_0) = \delta(\mathbf{r}) \delta(\vartheta - \vartheta_0)$.

We also introduce the spatial Fourier transform

$$\tilde{\mathbb{P}}(\mathbf{k}, \vartheta, t | \vartheta_0) = \int d^2 r \exp(-i\mathbf{k} \cdot \mathbf{r}) \mathbb{P}(\mathbf{r}, \vartheta, t | \vartheta_0), \quad (\text{SM9})$$

with corresponding e.o.m.

$$\begin{aligned} \partial_t \tilde{\mathbb{P}} &= -\partial_\vartheta [(\omega - \gamma \sin \vartheta) \tilde{\mathbb{P}}] + D_{\text{rot}} \partial_\vartheta^2 \tilde{\mathbb{P}} - i\mathbf{k} \cdot \mathbf{V} \tilde{\mathbb{P}} - D_\perp k^2 \tilde{\mathbb{P}} - (D_\parallel - D_\perp) (\mathbf{u}^\parallel \cdot \mathbf{k})^2 \tilde{\mathbb{P}} \\ &=: (\mathcal{L} + \delta \mathcal{L}_\mathbf{k}) \tilde{\mathbb{P}}. \end{aligned} \quad (\text{SM10})$$

Here the operator \mathcal{L} encodes the motion of the angle, while $\delta \mathcal{L}_\mathbf{k} = -i\mathbf{k} \cdot \mathbf{V} - D_\perp k^2 - (D_\parallel - D_\perp) (\mathbf{u}^\parallel \cdot \mathbf{k})^2$ describes the coupling to the translational dynamics. The formal solution is thus $\tilde{\mathbb{P}}(\mathbf{k}, \vartheta, t | \vartheta_0) = \exp[(\mathcal{L} + \delta \mathcal{L}_\mathbf{k})t] \delta(\vartheta - \vartheta_0)$. From this quantity the intermediate scattering function (ISF) $F(\mathbf{k}, t) = \langle \exp(-i\mathbf{k} \cdot \Delta \mathbf{r}(t)) \rangle$ is obtained in the stationary state by averaging over the initial angle and summing over the final one

$$F(\mathbf{k}, t) = \int_0^{2\pi} d\vartheta \int_0^{2\pi} d\vartheta_0 \tilde{\mathbb{P}}(\mathbf{k}, \vartheta, t | \vartheta_0) p^{\text{st}}(\vartheta_0) = \int_0^{2\pi} d\vartheta \exp[(\mathcal{L} + \delta \mathcal{L}_\mathbf{k})t] p^{\text{st}}(\vartheta), \quad (\text{SM11})$$

where $p^{\text{st}}(\cdot)$ is the non-trivial distribution of the orientation in the steady state. We will derive low-order spatial moments by series expansion in powers of the wavevector \mathbf{k} .

It is favorable to rely on the isomorphism of periodic square-integrable functions $f(\vartheta) \in L^2[0, 2\pi]$ and abstract states $|f\rangle \in \mathcal{H}$ [4]. The relation is made explicit by introducing generalized eigenstates $|\vartheta\rangle$ such that $f(\vartheta) = \langle \vartheta | f \rangle$. For this to hold we require

$$\langle f | g \rangle = \int_0^{2\pi} d\vartheta f(\vartheta)^* g(\vartheta) = \int_0^{2\pi} d\vartheta \langle f | \vartheta \rangle \langle \vartheta | g \rangle, \quad (\text{SM12})$$

for all $f, g \in L^2[0, 2\pi]$. We therefore infer the completeness relation

$$\int_0^{2\pi} d\vartheta |\vartheta\rangle \langle \vartheta| = \mathbb{1}. \quad (\text{SM13})$$

Furthermore from

$$\mathbb{1}^2 = \int_0^{2\pi} d\vartheta \int_0^{2\pi} d\vartheta_0 |\vartheta\rangle\langle\vartheta|\vartheta_0\rangle\langle\vartheta_0| \stackrel{!}{=} \mathbb{1}, \quad (\text{SM14})$$

we conclude the generalized orthogonality

$$\langle\vartheta|\vartheta_0\rangle = \delta(\vartheta - \vartheta_0). \quad (\text{SM15})$$

We write $\{|n\rangle : n \in \mathbb{Z}\}$ for the standard orthonormal basis (ONB) in \mathcal{H} with real-space representation $\langle\vartheta|n\rangle = \exp(in\vartheta)/\sqrt{2\pi}$. We define the (non-Hermitian) operator \mathcal{L} in \mathcal{H} via its matrix elements $\langle m|\mathcal{L}n\rangle$ [69] of the Fokker-Planck operator [3]

$$\mathcal{L}_{mn} = \langle m|\mathcal{L}n\rangle = \int_0^{2\pi} \frac{d\vartheta}{2\pi} e^{-im\vartheta} \mathcal{L} e^{in\vartheta} = (-D_{\text{rot}}m^2 - im\omega)\delta_{mn} + \frac{\gamma}{2}m(\delta_{m,n+1} - \delta_{m,n-1}). \quad (\text{SM16})$$

In particular the matrix representation becomes tridiagonal. We solve for right and left eigenstates of the Fokker-Planck operator

$$\mathcal{L}|r_\lambda\rangle = -\lambda|r_\lambda\rangle, \quad \mathcal{L}^\dagger|l_\lambda\rangle = -\lambda^*|l_\lambda\rangle, \quad (\text{SM17})$$

by expansion in the ONB

$$|r_\lambda\rangle = \sum_n |n\rangle\langle n|r_\lambda\rangle, \quad |l_\lambda\rangle = \sum_n |n\rangle\langle n|l_\lambda\rangle. \quad (\text{SM18})$$

Then the expansion coefficients $\langle n|r_\lambda\rangle$ and $\langle n|l_\lambda\rangle$ diagonalize the matrix $\langle m|\mathcal{L}n\rangle$

$$\sum_n \langle m|\mathcal{L}n\rangle\langle n|r_\lambda\rangle = -\lambda\langle m|r_\lambda\rangle, \quad \sum_n \langle m|\mathcal{L}^\dagger n\rangle\langle n|l_\lambda\rangle = -\lambda\langle m|l_\lambda\rangle. \quad (\text{SM19})$$

In particular, the left and right eigenstates can be chosen to be orthonormal and we assume that they span the entire Hilbert space

$$\langle l_\mu|r_\lambda\rangle = \delta_{\mu\lambda}, \quad \sum_\lambda |r_\lambda\rangle\langle l_\lambda| = \mathbb{1}, \quad (\text{SM20})$$

where \sum_λ means that we are summing over all eigenspaces. By conservation of probability the left eigenstate to eigenvalue 0 is trivial: $\langle l_0| = \langle 0|$, see Eq. (SM16). The corresponding right eigenstate $|r_0\rangle$ is the stationary state with real space representation $\langle\vartheta|r_0\rangle = p^{\text{st}}(\vartheta)$, where the normalizing factor is chosen such that $\langle l_0|r_0\rangle = 1$.

The angular propagator $P(\vartheta, t|\vartheta_0)$ encoding the probability to find an angle ϑ at lag time t given the initial orientation at time $t = 0$ was ϑ_0 can then be written conveniently in abstract form as

$$P(\vartheta, t|\vartheta_0) = e^{\mathcal{L}t}\delta(\vartheta - \vartheta_0) = \sum_\lambda e^{-\lambda t}\langle\vartheta|r_\lambda\rangle\langle l_\lambda|\vartheta_0\rangle = \langle\vartheta|\sum_\lambda e^{\mathcal{L}t}r_\lambda\rangle\langle l_\lambda|\vartheta_0\rangle = \langle\vartheta|e^{\mathcal{L}t}\vartheta_0\rangle. \quad (\text{SM21})$$

Perturbation theory

The full propagator $\tilde{\mathbb{P}}(\mathbf{k}\vartheta t|\vartheta_0)$ solves the Fokker-Planck equation

$$\partial_t \tilde{\mathbb{P}} = (\mathcal{L} + \delta\mathcal{L}_{\mathbf{k}})\tilde{\mathbb{P}}, \quad (\text{SM22})$$

with the perturbation

$$\begin{aligned} \delta\mathcal{L}_{\mathbf{k}} &= -i\mathbf{k} \cdot \mathbf{V} - D_\perp k^2 - (D_\parallel - D_\perp)(\mathbf{u}^\parallel \cdot \mathbf{k})^2 \\ &= -ik_x v \cos\vartheta - ik_y v \sin\vartheta + ik_x v_1 \sin(\varphi_H + \vartheta) - ik_y v_1 \cos(\vartheta_H + \vartheta) + ik_x v_2 \sin[2(\varphi_H + \vartheta)] + ik_y v_2 \cos[2(\varphi_H + \vartheta)] \\ &\quad + iv_3 k_y - \frac{D_\parallel - D_\perp}{2} [(k_x^2 - k_y^2) \cos(2(\varphi_H + \vartheta)) + 2k_x k_y \sin(2(\varphi_H + \vartheta))] - \frac{D_\parallel + D_\perp}{2} k^2. \end{aligned} \quad (\text{SM23})$$

In the following we discard all terms due to translational motion and keep only

$$\delta\mathcal{L}_{\mathbf{k}} = -iv\mathbf{k} \cdot \mathbf{u} = -ik_x v \cos\vartheta - ik_y v \sin\vartheta, \quad (\text{SM24})$$

with corresponding matrix elements

$$(\delta\mathcal{L}_{\mathbf{k}})_{mn} = \langle m|\delta\mathcal{L}_{\mathbf{k}}n\rangle = -\frac{ik_x v}{2}(\delta_{m,n+1} + \delta_{m,n-1}) - \frac{k_y v}{2}(\delta_{m,n+1} - \delta_{m,n-1}). \quad (\text{SM25})$$

The formal solution is then given by

$$\tilde{\mathbb{P}}(\mathbf{k}\vartheta t|\vartheta_0) = e^{(\mathcal{L}+\delta\mathcal{L}_{\mathbf{k}})t}\delta(\vartheta - \vartheta_0) = \langle\vartheta|e^{(\mathcal{L}+\delta\mathcal{L}_{\mathbf{k}})t}\vartheta_0\rangle. \quad (\text{SM26})$$

Then the intermediate scattering function in the stationary state is obtained as

$$F(\mathbf{k}, t) = \int_0^{2\pi} d\vartheta \int_0^{2\pi} d\vartheta_0 \langle l_0|\vartheta\rangle \langle\vartheta|e^{(\mathcal{L}+\delta\mathcal{L}_{\mathbf{k}})t}\vartheta_0\rangle \langle\vartheta_0|r_0\rangle = \langle l_0|e^{(\mathcal{L}+\delta\mathcal{L}_{\mathbf{k}})t}r_0\rangle. \quad (\text{SM27})$$

We use the Dyson representation [4] for the time evolution operator

$$e^{(\mathcal{L}+\delta\mathcal{L}_{\mathbf{k}})t} = e^{\mathcal{L}t} + \int_0^t ds e^{\mathcal{L}(t-s)}\delta\mathcal{L}_{\mathbf{k}}e^{(\mathcal{L}+\delta\mathcal{L}_{\mathbf{k}})s}, \quad (\text{SM28})$$

and expand to second order in the perturbation

$$e^{(\mathcal{L}+\delta\mathcal{L}_{\mathbf{k}})t} = e^{\mathcal{L}t} + \int_0^t ds e^{\mathcal{L}(t-s)}\delta\mathcal{L}_{\mathbf{k}}e^{\mathcal{L}s} + \int_0^t ds \int_0^s du e^{\mathcal{L}(t-s)}\delta\mathcal{L}_{\mathbf{k}}e^{\mathcal{L}(s-u)}\delta\mathcal{L}_{\mathbf{k}}e^{\mathcal{L}u} + O(\delta\mathcal{L}_{\mathbf{k}})^3, \quad (\text{SM29})$$

and sandwich it between the states $\langle l_0|$ and $|r_0\rangle$. Note further that $\langle l_0|e^{\mathcal{L}t} = \langle e^{\mathcal{L}^\dagger t}l_0| = \langle l_0|$ by conservation of probability and $e^{\mathcal{L}t}|r_0\rangle = |r_0\rangle$ by the definition of the stationary state. This yields

$$\begin{aligned} F(\mathbf{k}, t) &= 1 + \int_0^t ds \langle l_0|e^{\mathcal{L}(t-s)}\delta\mathcal{L}_{\mathbf{k}}e^{\mathcal{L}s}r_0\rangle + \int_0^t ds \int_0^s du \langle l_0|e^{\mathcal{L}(t-s)}\delta\mathcal{L}_{\mathbf{k}}e^{\mathcal{L}(s-u)}\delta\mathcal{L}_{\mathbf{k}}e^{\mathcal{L}u}r_0\rangle + O(|\mathbf{k}|^3) \\ &= 1 + t\langle l_0|\delta\mathcal{L}_{\mathbf{k}}r_0\rangle + \sum_\lambda \int_0^t ds \int_0^s du \langle l_0|\delta\mathcal{L}_{\mathbf{k}}e^{\mathcal{L}(s-u)}r_\lambda\rangle \langle l_\lambda|\delta\mathcal{L}_{\mathbf{k}}r_0\rangle + O(|\mathbf{k}|^3) \\ &= 1 + t\langle l_0|\delta\mathcal{L}_{\mathbf{k}}r_0\rangle + \sum_\lambda \int_0^t ds \int_0^s du e^{-\lambda(s-u)} \langle l_0|\delta\mathcal{L}_{\mathbf{k}}r_\lambda\rangle \langle l_\lambda|\delta\mathcal{L}_{\mathbf{k}}r_0\rangle + O(|\mathbf{k}|^3) \\ &= 1 + t\langle l_0|\delta\mathcal{L}_{\mathbf{k}}r_0\rangle + \sum_\lambda \frac{e^{-\lambda t} + \lambda t - 1}{\lambda^2} \langle l_0|\delta\mathcal{L}_{\mathbf{k}}r_\lambda\rangle \langle l_\lambda|\delta\mathcal{L}_{\mathbf{k}}r_0\rangle + O(|\mathbf{k}|^3). \end{aligned} \quad (\text{SM30})$$

For the cumulant-generating function this implies

$$\begin{aligned} \ln F(\mathbf{k}, t) &= t\langle l_0|\delta\mathcal{L}_{\mathbf{k}}r_0\rangle + \sum_\lambda \frac{e^{-\lambda t} + \lambda t - 1}{\lambda^2} \langle l_0|\delta\mathcal{L}_{\mathbf{k}}r_\lambda\rangle \langle l_\lambda|\delta\mathcal{L}_{\mathbf{k}}r_0\rangle - \frac{t^2}{2} \langle l_0|\delta\mathcal{L}_{\mathbf{k}}r_0\rangle \langle l_0|\delta\mathcal{L}_{\mathbf{k}}r_0\rangle + O(|\mathbf{k}|^3) \\ &= t\langle l_0|\delta\mathcal{L}_{\mathbf{k}}r_0\rangle + \sum_{\lambda \neq 0} \frac{e^{-\lambda t} + \lambda t - 1}{\lambda^2} \langle l_0|\delta\mathcal{L}_{\mathbf{k}}r_\lambda\rangle \langle l_\lambda|\delta\mathcal{L}_{\mathbf{k}}r_0\rangle + O(|\mathbf{k}|^3). \end{aligned} \quad (\text{SM31})$$

On the other hand the cumulant expansion yields

$$\begin{aligned} \ln F(\mathbf{k}, t) &= \ln \langle \exp(i\mathbf{k} \cdot \Delta\mathbf{r}(t)) \rangle = \ln \left\langle 1 + i\mathbf{k} \cdot \Delta\mathbf{r}(t) - \frac{1}{2}[\mathbf{k} \cdot \Delta\mathbf{r}(t)]^2 + O(|\mathbf{k}|^3) \right\rangle \\ &= i\mathbf{k} \cdot \langle \Delta\mathbf{r}(t) \rangle - \frac{1}{2} \{ \langle [\mathbf{k} \cdot \Delta\mathbf{r}(t)]^2 \rangle - [\langle \mathbf{k} \cdot \Delta\mathbf{r}(t) \rangle]^2 \}. \end{aligned} \quad (\text{SM32})$$

In particular, we read off the mean drift velocity along the direction $\mathbf{n} := \mathbf{k}/k$

$$\mathbf{n} \cdot \frac{d}{dt} \langle \Delta\mathbf{r}(t) \rangle = \frac{1}{k} \langle l_0|\delta\mathcal{L}_{\mathbf{k}}r_0\rangle, \quad (\text{SM33})$$

as well as the variance

$$\begin{aligned}\text{Var}[\mathbf{n} \cdot \Delta \mathbf{r}(t)] &= \langle [\mathbf{n} \cdot \Delta \mathbf{r}(t)]^2 \rangle - [\langle \mathbf{n} \cdot \Delta \mathbf{r}(t) \rangle]^2 \\ &= \frac{2}{k^2} \sum_{\lambda \neq 0} \frac{1 - \lambda t - e^{-\lambda t}}{\lambda^2} \langle l_0 | \delta \mathcal{L}_{\mathbf{k}} r_\lambda \rangle \langle l_\lambda | \delta \mathcal{L}_{\mathbf{k}} r_0 \rangle.\end{aligned}\quad (\text{SM34})$$

In particular for the corresponding diffusion coefficient

$$D_{\mathbf{n}} := \lim_{t \rightarrow \infty} \frac{1}{2} \frac{d}{dt} \text{Var}[\mathbf{n} \cdot \Delta \mathbf{r}(t)] = \frac{-1}{k^2} \sum_{\lambda \neq 0} \frac{1}{\lambda} \langle l_0 | \delta \mathcal{L}_{\mathbf{k}} r_\lambda \rangle \langle l_\lambda | \delta \mathcal{L}_{\mathbf{k}} r_0 \rangle.\quad (\text{SM35})$$

For short times the variance grows as t^2 since

$$\begin{aligned}\text{Var}[\mathbf{n} \cdot \Delta \mathbf{r}(t)] &= \frac{1}{k^2} t^2 \sum_{\lambda \neq 0} \langle l_0 | \delta \mathcal{L}_{\mathbf{k}} r_\lambda \rangle \langle l_\lambda | \delta \mathcal{L}_{\mathbf{k}} r_0 \rangle + O(t^3) \\ &= \frac{1}{k^2} t^2 \langle l_0 | \delta \mathcal{L}_{\mathbf{k}} \delta \mathcal{L}_{\mathbf{k}} r_0 \rangle - \frac{1}{k^2} t^2 \langle l_0 | \delta \mathcal{L}_{\mathbf{k}} r_0 \rangle \langle l_0 | \delta \mathcal{L}_{\mathbf{k}} r_0 \rangle + O(t^3).\end{aligned}\quad (\text{SM36})$$

Numerical results for the eigenspectrum

Numerical results for the magnitude of the first non-trivial eigenvalue λ_1 for decreasing noise are shown in Fig. SM2 on double-logarithmic scales. For $D_{\text{rot}} \rightarrow 0$ they approach finite values which become smaller and smaller as the separation parameter $\epsilon = (\gamma - \omega)/\omega$ decreases. Empirically we find that $\lambda_n \propto \sqrt{\epsilon}$ in the limit of vanishing noise. The shapes of the curves above the bifurcation become identical as the bifurcation is approached, $\epsilon \rightarrow 0$, and similarly below the bifurcation. This observation holds generally for the low-lying eigenvalues $\lambda_n, n = 1, 2, \dots$. The curves can be superimposed upon shifting vertically by their low-noise values and proper rescaling of the rotational diffusion constant. We achieve data collapse using the reduced rotational diffusion coefficient $\hat{D}_{\text{rot}} \propto |\epsilon|^{-3/2} D_{\text{rot}}$ suggesting the scaling law

$$\lambda_n/\omega = \sqrt{2|\epsilon|} \Lambda_{n,\pm}(\hat{D}_{\text{rot}}), \quad (\text{SM37})$$

with dimensionless scaling functions $\Lambda_{n,\pm}(\cdot)$ for $\epsilon \gtrless 0$ (it turns out that the factor 2 in the square root renders $\Lambda_{n,+}(\hat{D}_{\text{rot}} \rightarrow 0) = n$).

The inset of Fig. SM2 exhibits the scaling behavior in the vicinity of the bifurcation for small noise. By construction both scaling functions saturate for small reduced rotational diffusion coefficient $\hat{D}_{\text{rot}} \ll 1$, while for large $\hat{D}_{\text{rot}} \gg 1$ they behave as a power law with an exponent of $1/3$:

$$\Lambda_{n,\pm}(\hat{D}_{\text{rot}}) \sim C_n \hat{D}_{\text{rot}}^{1/3} \quad \text{for } \hat{D}_{\text{rot}} \rightarrow \infty, \quad (\text{SM38})$$

with constants C_n independent of the sign of ϵ . In the next subsection the scaling behavior of the low-noise limit as well as the proper choice of \hat{D}_{rot} is rationalized in terms of a harmonic-oscillator picture.

Harmonic approximation

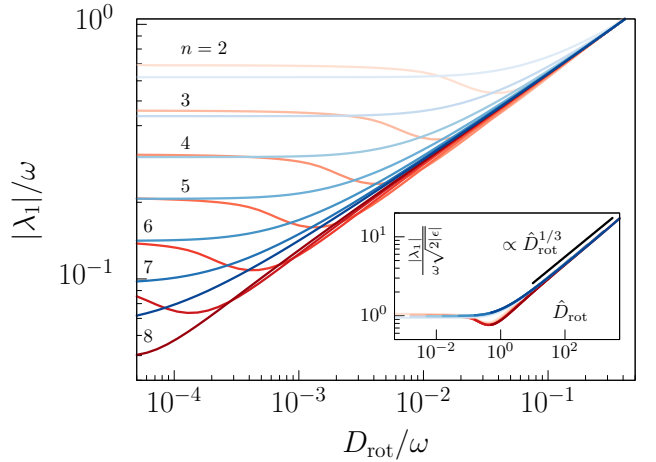


Fig. SM2. Absolute value of the first non-vanishing eigenvalue, $|\lambda_1|$, vs. diffusivity D_{rot} for decreasing separation parameter $\epsilon = (\gamma - \omega)/\omega = \pm 10^{-n/3}, n = 2, \dots, 8$. The red lines are for $\epsilon > 0$, while blue ones correspond to $\epsilon < 0$. The color becomes darker as the absolute value of the separation parameter approaches zero. Inset: Rescaled eigenvalues $|\lambda_1|/\omega \sqrt{2|\epsilon|}$ vs. reduced rotational diffusion coefficient $\hat{D}_{\text{rot}} := |\epsilon|^{-3/2} D_{\text{rot}}/\omega$. The straight solid line indicates a power law $\propto \hat{D}_{\text{rot}}^{1/3}$ and serves as guide to the eye.

We rewrite the stochastic e.o.m. in terms of an effective potential $U(\vartheta)$

$$\dot{\vartheta} = -\frac{D_{\text{rot}}}{k_B T} \partial_{\vartheta} U + \zeta(t). \quad (\text{SM39})$$

Here $D_{\text{rot}}/k_B T$ is then the mobility for the overdamped motion of the angle and the potential reads

$$\frac{D_{\text{rot}}}{k_B T} U(\vartheta) = -\omega \vartheta - \gamma \cos \vartheta. \quad (\text{SM40})$$

For $\gamma \geq \omega$ the potential displays a minimum at $\vartheta_* \in [0, \pi/2]$ with $\sin \vartheta_* = \omega/\gamma$ while a maximum is displayed at $\pi - \vartheta_* \in [\pi/2, \pi]$, see Fig. SM3 for illustration. Let's make a harmonic approximation for the potential close to the minimum,

$$\frac{D_{\text{rot}}}{k_B T} U(\vartheta) = \frac{D_{\text{rot}}}{k_B T} U(\vartheta_*) + \frac{(\vartheta - \vartheta_*)^2}{2} \gamma \cos \vartheta_* + O(\vartheta - \vartheta_*)^3. \quad (\text{SM41})$$

For the stochastic e.o.m. this results in a linear Langevin equation

$$\dot{\vartheta} = -\frac{1}{\tau} (\vartheta - \vartheta_*) + \zeta(t), \quad (\text{SM42})$$

with relaxation rate

$$\frac{1}{\tau} = \gamma \cos \vartheta_* = \sqrt{\gamma^2 - \omega^2}. \quad (\text{SM43})$$

The eigenvalues of the overdamped harmonic oscillator are simply

$$\lambda_n = \frac{1}{\tau} n. \quad (\text{SM44})$$

The picture of the harmonic oscillator is expected to be valid for the low eigenvalues if the escape rate for diffusing over the barrier is small compared to the relaxation rate. For large barriers $\Delta U := U(\pi - \vartheta_*) - U(\vartheta_*)$ the escape is exponentially suppressed. $\propto \exp(-\Delta U/k_B T)$, by Kramers' law, correspondingly we require that the barrier is high with respect to the thermal energy

$$\begin{aligned} 1 \ll \frac{\Delta U}{k_B T} &= \frac{1}{k_B T} [U(\pi - \vartheta_*) - U(\vartheta_*)] \\ &= \frac{1}{D_{\text{rot}}} [2\omega \arcsin(\omega/\gamma) - \pi\omega + 2\sqrt{\gamma^2 - \omega^2}]. \end{aligned} \quad (\text{SM45})$$

The condition is certainly fulfilled for $D_{\text{rot}} \rightarrow 0$ for fixed $\gamma > \omega$. Here we want to investigate the scaling limit of $D_{\text{rot}}/\omega \rightarrow 0$ and $\epsilon := (\gamma - \omega)/\omega \rightarrow 0$. Then upon series expansion the condition of high barrier translates to

$$1 \ll \frac{\Delta U}{k_B T} = \frac{4\sqrt{2}}{3} \frac{\omega}{D_{\text{rot}}} \epsilon^{3/2} + O(\dots). \quad (\text{SM46})$$

This is the condition, Eq. (14), of the main text.

Matrix elements of the harmonic oscillator

For small D_{rot} and $\gamma > \omega$ we perform the harmonic oscillator approximation around the minimum ϑ_* , $x := \vartheta - \vartheta_*$

$$\begin{aligned} \mathcal{L} &= D_{\text{rot}} \frac{\partial^2}{\partial \vartheta^2} - \frac{\partial}{\partial \vartheta} (\omega - \gamma \sin \vartheta) = D_{\text{rot}} \frac{\partial^2}{\partial x^2} - \frac{\partial}{\partial x} [\omega - \gamma \sin(\vartheta_* + x)] \\ &\approx D_{\text{rot}} \frac{\partial^2}{\partial x^2} - \frac{\partial}{\partial x} (\omega - \gamma \sin \vartheta_* - x\gamma \cos \vartheta_*). \end{aligned} \quad (\text{SM47})$$

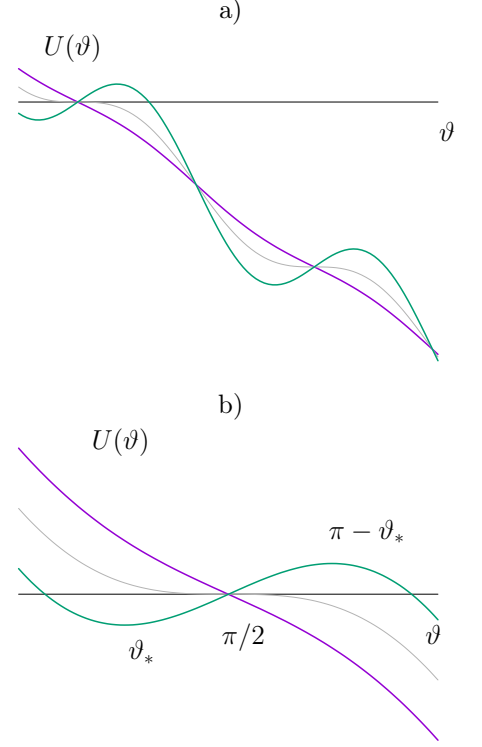


Fig. SM3. a) Titled washboard potential $U(\vartheta)$. b) Zoom close to the classical bifurcation.

Since $\gamma \sin \vartheta_* = \omega$ and $\gamma \cos \vartheta_* = \sqrt{\gamma^2 - \omega^2} =: 1/\tau$ this simplifies to

$$\mathcal{L} = D_{\text{rot}} \frac{\partial^2}{\partial x^2} + \frac{\partial}{\partial x} \left(\frac{x}{\tau} \right). \quad (\text{SM48})$$

This Fokker-Planck operator corresponds to the effective potential

$$\frac{D_{\text{rot}} U(x)}{k_B T} = \frac{x^2}{2\tau}. \quad (\text{SM49})$$

The angular oscillator width $\langle (\vartheta - \vartheta_*)^2 \rangle^{1/2} = \sqrt{\langle x^2 \rangle} = \sqrt{D_{\text{rot}} \tau}$ quantifies the mean-square fluctuations. For $D_{\text{rot}} \rightarrow 0$ the eigenfunctions become more and more localized.

For the perturbation we expand also to linear order

$$\begin{aligned} \delta \mathcal{L}_{\mathbf{k}} &= -ik_x v \cos \vartheta - ik_y v \sin \vartheta = -ik_x v \cos(\vartheta_* + x) - ik_y v \sin(\vartheta_* + x) \\ &= -ik_x v \cos \vartheta_* - ik_y v \sin \vartheta_* + (ik_x v \sin \vartheta_* - ik_y v \cos \vartheta_*) x + O(x^2). \end{aligned} \quad (\text{SM50})$$

Thus to leading order only the diagonal components are non-vanishing

$$\langle l_\mu | \delta \mathcal{L}_{\mathbf{k}} | r_\lambda \rangle = (-ik_x v \cos \vartheta_* - ik_y v \sin \vartheta_*) \delta_{\mu\lambda} + O(\cdot). \quad (\text{SM51})$$

This yields for the mean drift

$$\mathbf{n} \cdot \frac{d}{dt} \langle \Delta \mathbf{r}(t) \rangle = \frac{1}{k} \langle l_0 | \delta \mathcal{L}_{\mathbf{k}} | r_0 \rangle \rightarrow (-in_x v \cos \vartheta_* - in_y v \sin \vartheta_*), \quad (\text{SM52})$$

with $\mathbf{n} = \mathbf{k}/k$. This reproduces the classical result.

The variance $\text{Var}_{\mathbf{n}}[\Delta \mathbf{r}(t)]$ vanishes as $D_{\text{rot}} \rightarrow 0$. To obtain the leading order we need to evaluate the matrix elements $\langle l_\mu | x | r_\lambda \rangle$ for $\mu \neq \lambda$. The fastest way is to use the gauge transformation to map the Fokker-Planck operator to a Schrödinger Hamiltonian [3] Define the Hamiltonian by the gauge transform

$$\begin{aligned} \mathcal{H} &= -e^{U(x)/2k_B T} \mathcal{L} e^{-U(x)/2k_B T} = -e^{x^2/4D_{\text{rot}}\tau} \mathcal{L} e^{-x^2/4D_{\text{rot}}\tau} \\ &= -D_{\text{rot}} \frac{\partial^2}{\partial x^2} + \frac{x^2}{4D_{\text{rot}}\tau^2} - \frac{1}{2\tau}, \end{aligned} \quad (\text{SM53})$$

which is Hermitian in $L^2(\mathbb{R})$. Adjoining yields

$$\mathcal{H} = -e^{-U(x)/2k_B T} \mathcal{L}^\dagger e^{U(x)/2k_B T}. \quad (\text{SM54})$$

We substitute $D_{\text{rot}} \mapsto \hbar^2/2m, 1/2D_{\text{rot}}\tau^2 \mapsto m\omega^2$ and find the shifted harmonic oscillator

$$\mathcal{H} = \frac{\hbar^2}{2m} \frac{\partial^2}{\partial x^2} + \frac{m\omega^2}{2} x^2 - \frac{\hbar\omega}{2}, \quad (\text{SM55})$$

with eigenvalues $\lambda_n = n\hbar\omega = n/\tau$. In particular the quantum oscillator length $\sqrt{\hbar/2m\omega}$ maps to the angular oscillator width $\sqrt{D_{\text{rot}}\tau}$. The matrix elements of x are thus expected to be of order $\sqrt{D_{\text{rot}}\tau}$

The corresponding mapping for the eigenfunctions is then

$$r_n(x) = e^{-U(x)/2k_B T} \psi_n(x), \quad (\text{SM56})$$

$$l_n(x) = e^{U(x)/2k_B T} \psi_n(x), \quad (\text{SM57})$$

with $\psi_n(x)$ the eigenfunctions of \mathcal{H} . The matrix elements of an operator \mathcal{V} are obtained as

$$\langle l_m | \mathcal{V} r_n \rangle = \int dx l_m(x)^* \mathcal{V} r_n(x) = \int dx \psi_m(x)^* [e^{U(x)/2k_B T} \mathcal{V} e^{-U(x)/2k_B T}] \psi_n(x). \quad (\text{SM58})$$

For the case of $\mathcal{V} = x$ the exponentials cancel, and we read off (with harmonic oscillator creation and annihilation operators a, a^\dagger)

$$\begin{aligned} \langle l_m | x | r_n \rangle &= \langle \psi_m | x | \psi_n \rangle = \langle \psi_m | \sqrt{\frac{\hbar}{2m\omega}} (a^\dagger + a) | \psi_n \rangle \\ &= \sqrt{\frac{\hbar}{2m\omega}} (\delta_{m,n+1} \sqrt{n+1} + \delta_{m,n-1} \sqrt{n}) \mapsto \sqrt{D_{\text{rot}}\tau} (\delta_{m,n+1} \sqrt{n+1} + \delta_{m,n-1} \sqrt{n}). \end{aligned} \quad (\text{SM59})$$

We thus read off the relevant matrix elements for the variance/diffusion coefficient

$$\langle l_0 | \delta \mathcal{L}_{\mathbf{k}r\lambda} \rangle = \langle l_\lambda | \delta \mathcal{L}_{\mathbf{k}r0} \rangle = iv \sqrt{D_{\text{rot}} \tau} (k_x \sin \vartheta_* - k_y \cos \vartheta_*) \delta_{\lambda,1}. \quad (\text{SM60})$$

The picture of the harmonic oscillator is valid only for $\hat{D}_{\text{rot}} \ll 1$. In this regime the formulas for the variance and diffusion simplify since only a single term contributes

$$\begin{aligned} \text{Var}[\mathbf{n} \cdot \Delta \mathbf{r}(t)] &= \frac{2}{k^2} \sum_{\lambda \neq 0} \frac{1 - \lambda t - e^{-\lambda t}}{\lambda^2} \langle l_0 | \delta \mathcal{L}_{\mathbf{k}r\lambda} \rangle \langle l_\lambda | \delta \mathcal{L}_{\mathbf{k}r0} \rangle \\ &= 2 \left(\frac{t}{\tau} - 1 + e^{-t/\tau} \right) (v\tau)^2 D_{\text{rot}} \tau (n_x \sin \vartheta_* - n_y \cos \vartheta_*)^2, \end{aligned} \quad (\text{SM61})$$

and infer the associated long-time diffusion coefficient

$$D_{\mathbf{n}} = (v\tau)^2 D_{\text{rot}} (n_x \sin \vartheta_* - n_y \cos \vartheta_*)^2. \quad (\text{SM62})$$

In particular, for small $D_{\text{rot}} \ll \omega$, $D_0 \approx v^2 D_{\text{rot}} / 2\omega^2$ in the harmonic oscillator approximation

$$D_{\mathbf{n}} / D_0 = 2(\omega\tau)^2 (n_x \sin \vartheta_* - n_y \cos \vartheta_*)^2 \approx \frac{1}{\epsilon} (n_x \sin \vartheta_* - n_y \cos \vartheta_*)^2.$$

This result yields prefactors to the scaling law derived in the main text.

SUPPLEMENTARY FIGURE ON MEAN DRIFT VELOCITY

The mean drift velocity is evaluated directly from the stationary distribution

$$v \begin{pmatrix} \langle \cos \vartheta \rangle \\ \langle \sin \vartheta \rangle \end{pmatrix} = \int_0^{2\pi} v \begin{pmatrix} \cos \vartheta \\ \sin \vartheta \end{pmatrix} p^{\text{st}}(\vartheta) d\vartheta. \quad (\text{SM63})$$

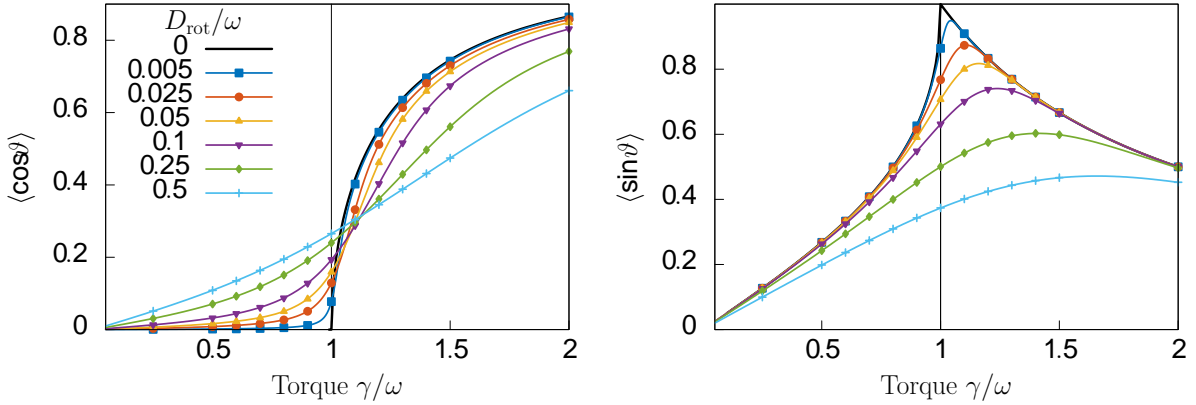


Fig. SM4. Mean drift velocity in the stationary state along the horizontal (left) and vertically against the field (right) as a function of the torque γ for various noise strength D_{rot} . Symbols correspond to simulation, full lines to numerical results.

The stationary distribution is known explicitly [3]

$$p^{\text{st}}(\vartheta) = \mathcal{N} e^{-U(\vartheta)/k_B T} \left[\int_{\vartheta}^{2\pi} e^{U(\bar{\vartheta})/k_B T} d\bar{\vartheta} + e^{[U(0) - U(2\pi)]/k_B T} \int_0^{\vartheta} e^{U(\bar{\vartheta})/k_B T} d\bar{\vartheta} \right], \quad (\text{SM64})$$

with the potential

$$\frac{D_{\text{rot}} U(\vartheta)}{k_B T} = -\omega \vartheta - \gamma \cos \vartheta. \quad (\text{SM65})$$

The normalization factor \mathcal{N} is fixed by imposing $\int_0^{2\pi} p^{\text{st}}(\vartheta) d\vartheta = 1$.

Numerical results for the average sine and cosine are displayed in Fig. SM4 but similar figures can also be found in Ref. [3].

SUPPLEMENTARY FIGURE ON INFLUENCE OF TRANSLATIONAL DIFFUSION ON THE RESONANCE

The techniques elaborated in the main text can be readily extended to include the additional drift terms and the translational diffusion in Eq. (SM5). The resonance for the full model emerges in the simultaneous limit of vanishing separation parameter and all noise terms approaching zero $D_{\text{rot}} \rightarrow 0, D_{\perp} \rightarrow 0, D_{\parallel} \rightarrow 0$ such that the ratios $D_{\perp}/D_{\text{rot}}, D_{\parallel}/D_{\text{rot}}$ remain fixed. Simulation as well as numerical results are displayed in Fig. SM5. Although diffusion broadens the resonance, the general picture remains valid.

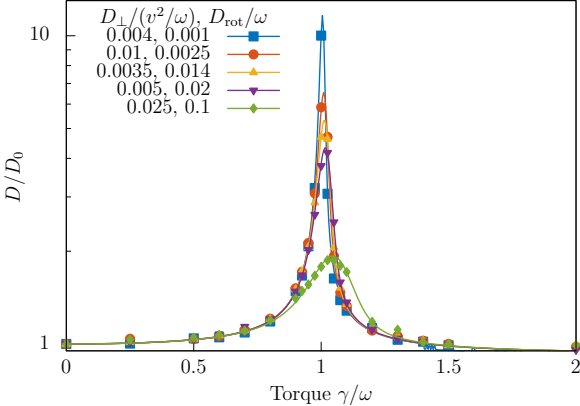


Fig. SM5. Diffusion coefficient D as a function of the torque γ for decreasing orientational diffusion coefficients D_{rot} and translational diffusion coefficients D_{\perp} ($D_{\parallel} = 2D_{\perp}$). Symbols correspond to simulation, full lines to numerical results. The values of the perpendicular component of the translational diffusivity D_{\perp} and rotational diffusivity D_{rot} are specified in the legend. The parallel component always is $D_{\parallel} = 2D_{\perp}$, for simplicity $\varphi_H = 0$, and we choose parameters such that $v_1 = v_2 = v_3/3 = v$.

BIBLIOGRAPHY

- [1] B. ten Hagen, F. Kümmel, R. Wittkowski, D. Takagi, H. Löwen, and C. Bechinger, Gravitaxis of asymmetric self-propelled colloidal particles, *Nature Communications* 5, 4829 (2014).
- [2] The use of the hydrodynamic expressions for active propulsion is controversial, see Ref. [6].
- [3] H. Risken, *The Fokker-Planck Equation* (Springer Berlin Heidelberg, 1989).
- [4] J. Sakurai and J. Napolitano, *Modern quantum mechanics*. San Fransico (CA: Addison-Wesley, 2011).
- [5] Since \mathcal{L} is non-Hermitian one has to carefully indicate whether operators act to the right or the left.
- [6] B. U. Felderhof, Comment on “Circular motion of asymmetric self-propelling particles”, *Physical Review Letters* 113 (2014); F. Kümmel, B. ten Hagen, R. Wittkowski, D. Takagi, I. Buttinoni, R. Eichhorn, G. Volpe, H. Löwen, and C. Bechinger, Kümmel et al. Reply:, *Physical Review Letters* 113, 029802 (2014).